Received: 7 July 2020 | Revised: 20 August 2020 | Accepted: 21 August 2020

DOI: 10.1002/kin.21422

WILEY

ARTICLE

Rate coefficients for the reactions of OH with butanols from 298 K to temperatures relevant for low-temperature combustion

Samantha L. Sime[1] | **Mark A. Blitz**[1,2] | **Paul W. Seakins**[1]

[1] School of Chemistry, University of Leeds, Leeds, LS2 9JT, UK

[2] National Centre for Atmospheric Science (NCAS), University of Leeds, Leeds, LS2 9JT, UK

Correspondence
Paul W. Seakins, School of Chemistry, University of Leeds, Leeds, LS2 9JT, UK.
Email: p.w.seakins@leeds.ac.uk

Abstract

Rate coefficients for the reactions of OH with n, s, and iso-butanol have been measured over the temperature range 298 to ~650 K. The rate coefficients display significant curvature over this temperature range and bridge the gap between previous low-temperature measurements with a negative temperature dependence and higher temperature shock tube measurements that have a positive temperature dependence. In combination with literature data, the following parameterizations are recommended:

$$k_{1,\mathrm{OH + n\text{-}butanol}}(T) = (3.8 \pm 10.4) \times 10^{-19} T^{2.48 \pm 0.37} \exp\left((840 \pm 161)/T\right) \mathrm{cm^3\ molecule^{-1}\ s^{-1}}$$

$$k_{2,\mathrm{OH + s\text{-}butanol}}(T) = (3.5 \pm 3.0) \times 10^{-20} T^{2.76 \pm 0.12} \exp\left((1085 \pm 55)/T\right) \mathrm{cm^3\ molecule^{-1}\ s^{-1}}$$

$$k_{3,\mathrm{OH + i\text{-}butanol}}(T) = (5.1 \pm 5.3) \times 10^{-20} T^{2.72 \pm 0.14} \exp\left((1059 \pm 66)/T\right) \mathrm{cm^3\ molecule^{-1}\ s^{-1}}$$

$$k_{4,\mathrm{OH + t\text{-}butanol}}(T) = (8.8 \pm 10.4) \times 10^{-22} T^{3.24 \pm 0.15} \exp\left((711 \pm 83)/T\right) \mathrm{cm^3\ molecule^{-1}\ s^{-1}}$$

Comparison of the current data with the higher shock tube measurements suggests that at temperatures of ~1000 K, the OH yields, primarily from decomposition of β-hydroxyperoxy radicals, are ~0.3 (*n*-butanol), ~0.3 (*s*-butanol) and ~0.2 (iso-butanol) with β-hydroxyperoxy decompositions generating OH, and a butene as the main products. The data suggest that decomposition of β-hydroxyperoxy radicals predominantly occurs via OH elimination.

KEYWORDS

butanols, curved Arrhenius, low-temperature combustion

1 | INTRODUCTION

The high-energy densities of liquid fuels is attractive, and in some cases essential, for transport and other applications. With careful production, liquid biofuels have the potential to reduce net CO_2 emissions[1-3] and oxygenated biofuels, such as ethanol, have additional benefits in reduced soot and NOx emissions.[4] Currently, primarily due to ease of manufacture, the major alcohol biofuel is ethanol, but butanols have advantages in terms of higher energy densities, better miscibility with fossil fuels in blends, and reduced corrosivity.[1,5–7]

Recent developments in engine technology such as homogeneous charge compression ignition (HCCI) and reaction-controlled compression ignition (RCCI)[8] have enhanced the focus on low-temperature combustion chemistry.[9-11] In HCCI and RCCI, auto-oxidation controls the ignition process and full optimization requires a detailed knowledge of the chemistry including the reaction kinetics of initiation processes, primarily reaction of the OH radical with the fuel.

There have been a number of studies of the reactions of OH with the butanols between 250 and 400 K (with a focus on atmospheric chemistry) and several shock tube studies, primarily by the Stanford group, at temperatures of 900-1200 K.[12-15]

$$OH + CH_3CH_2CH_2CH_2OH \rightarrow H_2O + C_4H_9O \quad (n-butanol) \qquad (R1)$$

$$OH + CH_3CH_2CH(OH)CH_3 \rightarrow H_2O + C_4H_9O \quad (s-butanol) \qquad (R2)$$

$$OH + (CH_3)_2CHCH_2OH \rightarrow H_2O + C_4H_9O \quad (i-butanol) \qquad (R3)$$

$$OH + (CH_3)_3COH \rightarrow H_2O + C_4H_9O\,(t-butanol) \qquad (R4)$$

However, there are no experimental measurements in between these temperature regimes in the region most relevant for low-temperature combustion, as exemplified in Figure 1, that shows literature data on the reaction of OH with *n*-butanol (R1). Data from the low-temperature studies[16,17] seem to demonstrate some slight curvature and while curvature has been predicted by several theoretical calculations,[21-25] to link the low- and high-temperature data,[12] the agreement with experiment can be poor.

OH can abstract H atoms from various positions in the butanols, including from the O−H bond; the possibilities for *n*-butanol are as follows:

$$OH + CH_3CH_2CH_2CH_2OH \rightarrow H_2O + CH_3CH_2CH_2CHOH \quad (\alpha-abstraction) \qquad (R1a)$$

$$\rightarrow H_2O + CH_3CH_2CHCH_2OH \quad (\beta-abstraction) \qquad (R1b)$$

$$\rightarrow H_2O + CH_3CHCH_2CH_2OH \quad (\gamma-abstraction) \qquad (R1c)$$

$$\rightarrow H_2O + CH_2CH_2CH_2CH_2OH \quad (\delta-abstraction) \qquad (R1d)$$

$$\rightarrow H_2O + CH_3CH_2CH_2CH_2O \quad (OH-abstraction). \qquad (R1e)$$

There have been a few direct studies[26-28] on the branching ratios of (R1) that confirm (R1a) as the dominant product between 300 and 600 K. McGillen et al[16] combined literature end-product analysis and structure activity relationships (SAR) to estimate site-specific rate coefficients. Limited site-specific data exist for other alcohols, that also suggest that abstraction at the α position dominates at room temperature, but that the reactions become less specific as temperature increases.[29,30] While the focus of this work is on the determination of the overall rate coefficients, our data do give some insights into branching ratios.

At high temperatures, there is potential for OH regeneration following abstraction at the β-position, for example, for *n*-butanol, (R1b) produces $CH_3CH_2CHCH_2OH$ that can decompose via two pathways:

$$CH_3CH_2CHCH_2OH \rightarrow OH + 1-butene \qquad (R5a)$$

$$\rightarrow CH_3 + CH_2{=}CHCH_2OH \qquad (R5b)$$

The shock-tube studies of Pang et al[12-14] and Stranic et al[15] were aware of this possibility, that is that measurements simply following the OH decay would be measuring the net rate of OH consumption. In the Pang et al studies, predictions of branching ratios and models of secondary chemistry were used to extract the total rate coefficient and in the study of Stranic et al isotopic labeling of the OH was used to ensure that the total rate coefficient was being measured. We will report on direct studies of OH regeneration in subsequent publications. Extending the direct

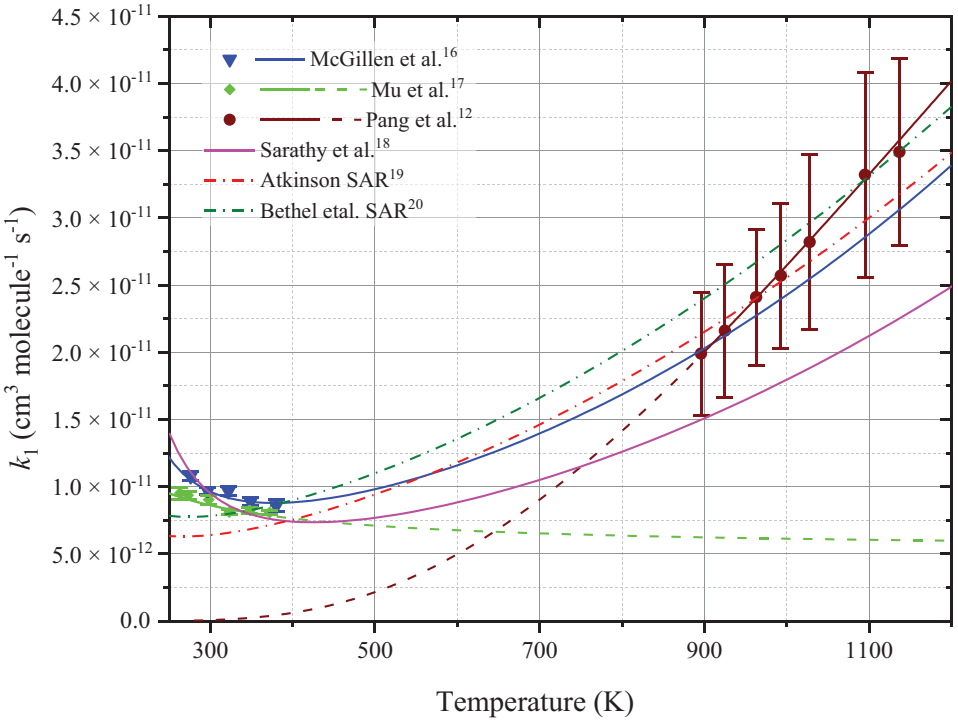

FIGURE 1 Temperature dependence of k_1 (OH + *n*-butanol) prior to this work. The temperature parameterizations of both experimental data[12,16,17] and SAR[18-20] have been extended over the full range of temperature to emphasize the discrepancy between low and high-temperature data [Color figure can be viewed at wileyonlinelibrary.com]

measurements of the rate coefficients allows some estimation of the validity of the indirect approach of Pang et al.

To summarize, the main objectives of this study are as follows:

- to obtain rate coefficients on the reaction of OH with the four butanol isomers at temperatures relevant for low-temperature combustion. This paper focuses primarily on n-, s-, and iso-butanol. Results on *t*-butanol will be presented, but a detailed consideration of the *t*-butanol system will be presented elsewhere.
- to demonstrate that the low- and high-temperature rate coefficient data that have different temperature dependencies in some cases can be bridged, and
- to provide more comprehensive datasets against which the demanding theoretical calculations can be tested. With only limited experimental data, such calculations are likely to be the main source of data on branching ratios.

2 | EXPERIMENTAL

The reaction of the butanols with OH was studied as a function of temperature using the laser flash photolysis-laser induced fluorescence method across the temperature range 298-715 K. The apparatus has been described in greater detail in previous studies.[31-33] The butanol reactants (all from Sigma-Aldrich), *n*-butanol, (≥99.4%), *s*-butanol (≥99.5%), *i*-butanol (≥99.0%) were made up into 10 L glass bulbs of alcohol diluted in nitrogen (N_2, BOC, oxygen free, 99.99%). For experiments requiring higher concentrations of butanol, the reagent was introduced via a bubbler. A reservoir of liquid reagent was placed in the bubbler, pressurized with a backing pressure of nitrogen to roughly 2 bar, and a flow of nitrogen over the top of the liquid was used to introduce butanol to the reaction cell. The vapor pressure of the butanol reservoir within the delivery bubbler was calculated based on the temperature of the room (measured via thermocouple prior to each trace being taken), and the concentration of reagent within the bubbler was then calculated as a percentage of the measured total pressure of the bubbler. Conducting experiments at 298 K using both bubbler and bulb methods of each butanol delivery consecutively allowed for corrections to be made on the bubbler delivery concentration. This correction introduces an additional uncertainty (<5%) in the rate coefficients measured using this method of butanol delivery.

The OH precursor (H_2O_2, Sigma-Aldrich, 50% w/w in H_2O), nitrogen bath gas, and butanol in nitrogen were flowed through calibrated mass flow controllers into a mixing manifold, before flowing into the six-way stainless steel reaction cell. When hydrogen peroxide makes contact

with the metal inside of the mass flow controller, subsequent decomposition results in the delivery of some oxygen into the system. This is expected to be around 2.5×10^{14} molecule cm^{-3} based on experiments conducted using the method described by Potter et al,[34] in which the residual oxygen present in the system is estimated based on the amount of OH recycled via O_2-dependent low pressure well-skipping. However, experiments in which larger concentrations of oxygen ($>10^{16}$ molecule cm^{-3}) were added showed no variation in rate coefficient in agreement with the work of McGillen et al.[16] The total gas flow was typically maintained around 1 or 2 L min^{-1}, for pressures of 30-40 or 85-90 Torr, respectively, to ensure a fresh sample of gas was used for each photolysis pulse. The pressure inside the reaction cell was maintained by a rotary pump throttled by a needle valve and monitored by a capacitance manometer. The reaction cell was heated by a series of cartridge heaters surrounding the cell, with the reaction cell temperature monitored by calibrated K-type thermocouples located near the reaction zone. Errors in the temperature, estimated by comparing the thermocouple readings around the reaction zone, were ±5 K at the lower end of the temperature range, rising to ±15 K at the highest temperatures.

OH radicals were generated by pulsed laser photolysis of hydrogen peroxide precursor (R6) in nitrogen buffer gas (N_2, BOC) at 248 nm using an excimer laser (KrF, Lambda Physik LPX 200), and monitored as a function of time by off-resonance laser-induced fluorescence. The photolysis laser fluence was measured prior to entrance into the reaction cell and was used to estimate the starting concentration of OH radicals produced during experiments. The laser repetition rate was typically 10 Hz (but was varied, between 2 and 10 Hz, with no impact on the measured rate coefficient), with a fluence of approximately 60-90 mJ cm^{-2} $pulse^{-1}$. This produces an approximate photon density of 1.1×10^{17} photons cm^{-2}, generating an initial [OH] of $\sim 1 \times 10^{12}$ molecule cm^{-3} from an initial H_2O_2 concentration of approximately 7×10^{13} molecule cm^{-3}.

$$H_2O_2 + h\upsilon\,(\lambda = 248\ \text{nm}) \rightarrow 2\bullet\text{OH} \qquad \text{(R6)}$$

The probe laser was a frequency-doubled Nd: YAG (Continuum Powerlite 8010) pumped dye laser (Spectra Physics PDL-3), operating on Rhodamine-6-G dye. The transition $A^2\Sigma\ (v' = 1) \leftarrow X^2\Pi\ (v'' = 0)$ was probed at 282 nm, and fluorescence was detected at 308 nm using a photomultiplier tube (CPM, Perkin-Elmer, C1943P) with a 308 nm filter (308 ± 5 nm, Barr Associates), and was detected perpendicular to the intersection of the photolysis and probe laser beams. A digital oscilloscope collected and integrated the fluorescence signal, before being transferred to a personal computer for analysis.

A time-dependent profile of OH fluorescence was built up by varying the time between the photolysis pulse and the probe pulse using a delay generator. Each experimental trace generated typically contained 200 time points, with 20 prezero time points to allow for averaging of a pretrigger background signal to subsequently be removed from the experimental trace. Kinetic traces were averaged for between 5 and 12 traces depending on signal quality. Reactions were carried out under pseudo–first-order conditions in which $[\text{butanol}] \gg [\text{OH}]_0$. Under these conditions, the signal intensity S_t at time t is proportional to the OH concentration $[\text{OH}]_t$, and the time dependence of S_t is given by

$$S_t = S_0 \times e^{-k' t} \qquad (1)$$

where S_0 represents signal intensity at time zero when the photolysis pulse occurs and k' is the pseudo–first-order rate coefficient related to the bimolecular rate coefficient, k_{bi}, via Equation (2),

$$k' = k_{\text{bi}}\ [\text{butanol}] + k_{\text{d}} \qquad (2)$$

where k_{bi} represents the total bimolecular rate coefficient for the reaction of butanol with OH and k_d represents other first-order loss processes for OH such as reaction with precursor and diffusive losses out of the observation region. Kinetic traces were fit using a nonlinear least squares fit to Equation (1) (Figure 2A).

Bimolecular rate coefficients are calculated from the slope of a plot of these pseudo–first-order rate constants k'_1 against varying concentration of butanol (E2), an example of which can be seen in Figure 2B. The intercept of the bimolecular reaction plot represents the k_d parameter, that is measured experimentally via a kinetic trace in the absence of any butanol.

3 | RESULTS AND DISCUSSION

Results and discussion are presented for each of the *n*-, *s*-, *i*-butanols followed by a brief intercomparison of all the butanols and how their rate coefficients and properties compare to other alcohols.

3.1 | *n*-Butanol

Results for the reaction of OH with *n*-butanol are presented in Table 1 and Figure 3. The measured bimolecular rate coefficients were independent of OH precursor (most experiments were carried out with H_2O_2, but a few used a urea/H_2O_2, although this was found to deliver

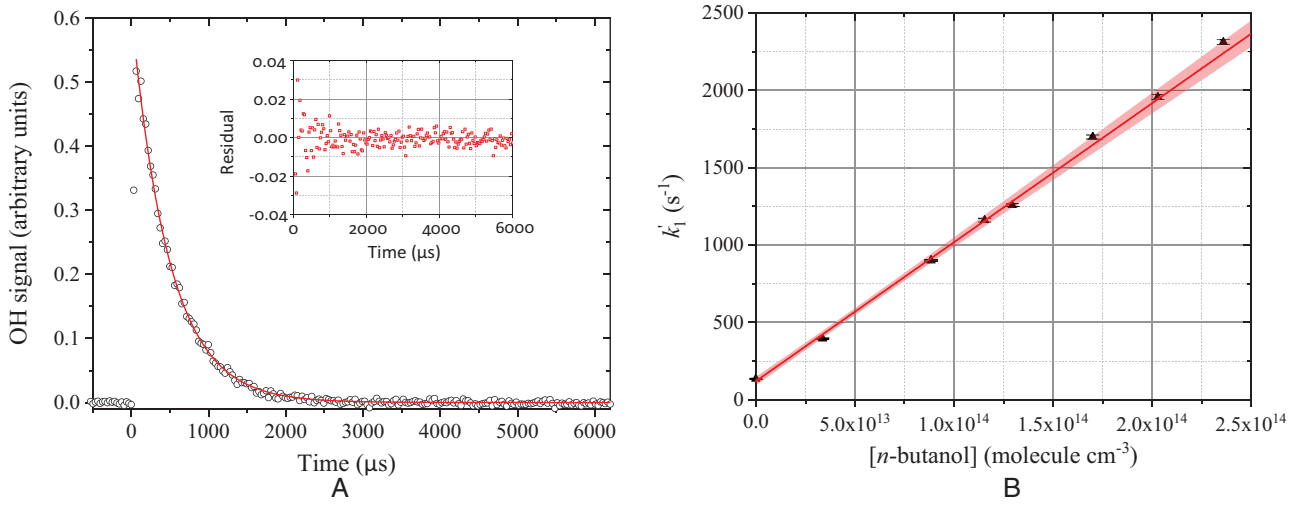

FIGURE 2 (A) Typical exponential OH decay curve. The red line is the fit to Equation (1) with the inset showing the residuals scattered around zero. Conditions: 35 Torr N_2, 298 K, [*n*-butanol] = 2.09×10^{14} molecule cm^{-3}. $k_1' = (2050 \pm 40)$ s^{-1}, where the error is 2σ. (B) Typical bimolecular plot. Conditions: 35 Torr N_2, 298 K. The resulting straight-line fit gives $k_1 = (8.98 \pm 0.32) \times 10^{-12}$ cm^3 molecule^{-1} s^{-1} where the error is 2σ. The 95% confidence limits are shown by the red area [Color figure can be viewed at wileyonlinelibrary.com]

TABLE 1 Summary of experimental conditions and bimolecular rate coefficients for the *n*-butanol and OH reaction

Temperature (K)	Pressure (Torr)	[*n*-Butanol] (molec cm^{-3})	k_1 (cm^3 molecule^{-1} s^{-1})	Temperature (K)	Pressure (Torr)	[*n*-Butanol] (molec cm^{-3})	k_1 (cm^3 molecule^{-1} s^{-1})
298	40	0.7-2.1	9.27 ± 0.14[a]	535	35	0.5-1.5	10.1 ± 0.46[b]
298	31	0.8-3.0	9.07 ± 0.16[a]	535	35	0.2-1.5	9.85 ± 0.45[b]
298	44	0.8-2.0	8.92 ± 0.22[a,d]	547	35	0.7-1.3	10.9 ± 0.50[b]
298	35	0.4-2.4	8.98 ± 0.16[a]	555	134	2.9-29.0	12.0 ± 1.2[b]
298	70	4.8-32.8	8.85 ± 0.89[c]	564	35	0.6-1.2	11.0 ± 0.51[b]
298	130	5.3-48.0	9.22 ± 0.92[c]	576	35	0.8-1.4	10.9 ± 0.50[b]
367	23	0.3-2.2	9.13 ± 0.42[b]	580	130	19.0-31.1	13.5 ± 1.4[c]
370	39	0.1-2.4	9.17 ± 0.42[b]	599	132	2.3-14.0	12.6 ± 1.3[c]
409	40	0.1-1.7	8.82 ± 0.51[b]	600	35	0.96-1.40	12.0 ± 0.72[b]
410	23	0.1-2.5	9.21 ± 0.43[b]	650	131	10.0-15.0	13.2 ± 1.3[c]
449	40	0.3-1.7	9.51 ± 0.44[b]	670	134	8.5-18.0	14.8 ± 1.5[c]
450	33	0.3-1.5	8.84 ± 0.41[b,d]	693	135	10.0-20.0	15.0 ± 1.5[c]
490	41	0.2-1.4	10.2 ± 0.54[b]	715	135	12.3-17.0	14.4 ± 1.4[c]
494	35	0.8-1.5	9.50 ± 0.44[b]				

[a] Standard 1σ error,
[b] 6% error based on standard deviation of room temperature measurements,
[c] Reagent delivered by bubbler, error increased to 10%,
[d] – $[O_2] = 1 \times 10^{16}$ molecule cm^{-3}.

more oxygen), added O_2 (at 298 K) and LIF scheme (most experiments used off-resonant detection, but particularly at higher [butanols] on resonant detection at 308 nm was used).

Table 2 compares our measured rate coefficients with a selection of literature values and predictions from SAR. The room temperature values range from 7.8 to 9.68×10^{-12} cm^3 molecule^{-1} s^{-1}. Issues around the reliable delivery of *n*-butanol to the reaction chamber are probably responsible for the spread in flash photolysis studies, for this reason, the recent work of McGillen et al,[16] where *n*-butanol deliver to the reaction chamber was monitored by both UV and IR spectroscopy, is likely to provide the most reliable comparison. Relative rate measurements should not be susceptible to the same uncertainties, but there will be a spread in values caused by uncertainties in the rate

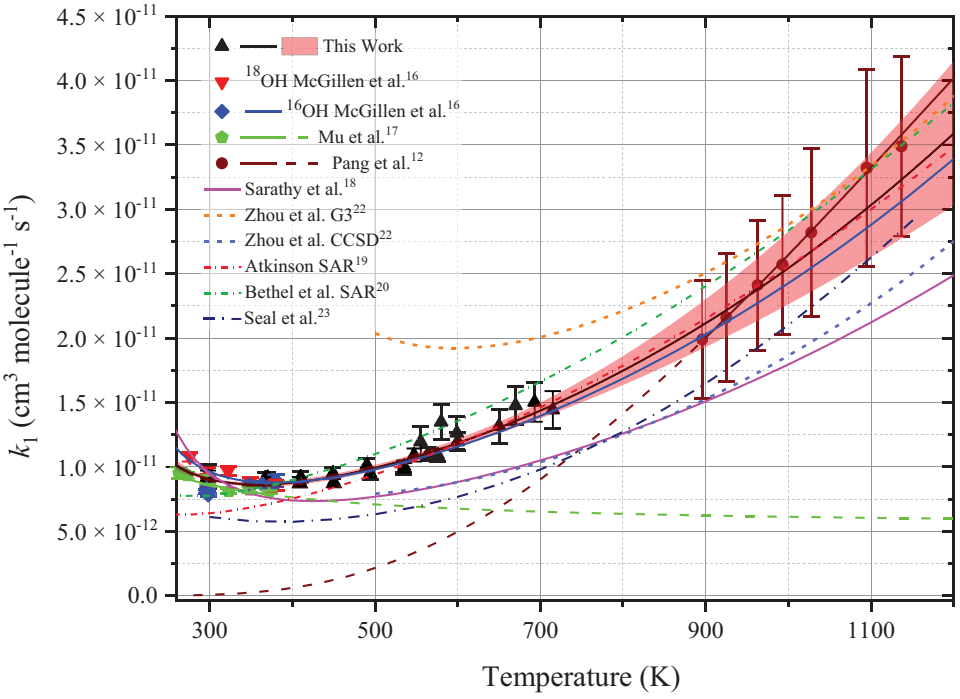

FIGURE 3 Temperature dependence for the rate coefficient for the reaction of OH and *n*-butanol incorporating this work, experimental data from Refs. 12, 16, and 17, and theoretical data from Refs. 18-20, 22, and 23 [Color figure can be viewed at wileyonlinelibrary.com]

coefficients of the reference compounds used, in addition to experimental errors.

McGillen et al[16] reported a small isotope enhancement (~10%) when they used ^{18}OH, suggesting that for *n*-butanol, there is a mechanism to recycle ^{16}OH. For alcohols, abstraction at the β-position followed by elimination of the hydroxyl group to form an alkene is the most obvious explanation; however, the effect persisted in the McGillen et al study even with the addition of large concentrations of O_2 that might be expected to intercept the β-hydroxyalkyl radical before OH elimination. Additionally, the effect appears to decrease with temperature in the McGillen et al study that seems to be incompatible with (R5a) as the source of the OH. No significant isotope effect was noted in our experiments when OD was used instead of OH.

Figure 3 shows that our measurements show an upturn in k_1 linking the lower temperature values of Mu and Mellouki,[17] and McGillen et al[16] (negative temperature dependence) with the high-temperature, positive temperature dependence results of Pang et al.[12] Curvature of k_1 had been predicted by theoretical calculations, but quantitative agreement with experimental values has been mixed. The calculations of Zhou et al[22] are strongly dependent on the ab initio method used and limited to temperatures above 500 K. At 500 K, they overestimate our measured value and extrapolation below 500 K (that may not be valid) is in poor agreement with experimental data. The more recent calculations of Seal et al[23] are in better agreement with experiment across the whole temperature range.

SARs are another way of predicting both total and site-selective rate coefficients. The original OH SAR of Atkinson[19] were known to perform badly for oxygenated species and were revised by Bethel et al.[20] The SAR of Bethel et al leads to an improved agreement at room temperature, but these relatively simple SAR are unable to capture the complex temperature dependence of the butanol systems. The branching ratios predicted by theoretical calculations and SAR differ significantly, and we return to this topic later in the discussion.

Combining the data of McGillen et al[16] and Pang et al[12] with this work yields the resultant modified Arrhenius parameterization that can be used to tune future theoretical calculations and SAR:

$$k_1(T) = (3.8 \pm 10.4) \times 10^{-19} T^{2.48\pm0.37} \exp\left((840 \pm 161)/T\right) \text{ cm}^3 \text{ molecule}^{-1} \text{ s}^{-1}.$$

3.2 | *s*-Butanol

Temperature-dependent rate coefficients for the reaction of OH with *s*-butanol (k_2) are shown in Table 3 and Figure 4. Our values show a clear decrease in k_2 between 300 and 370 K, beyond this minimum in k_2 around 370-420 K, k_2 gradually increases with temperature.

TABLE 2 Comparison of k_1 with literature data

Reference	Temperature (K)	Pressure (Torr)	Technique	$k_{1,298\ K}$ (cm^3 $molecule^{-1}$ s^{-1})	$k_1(T)$ (cm^3 $molecule^{-1}$ s^{-1})
Wallington and Kurylo[35]	296	25-50	FP-RF	8.31 ± 0.63	
Nelson et al[36]	298	760	PR-UV	7.8 ± 1.8	
	298	760	RR[a]	8.0 ± 2.6 (8.6 ± 2.1)[a]	
Mu and Mellouki[17]	253-372	30-300	LPF-LIF	8.47 ± 0.34	$(5.3 \pm 1.6) \times 10^{-12}\exp(146 \pm 92/T)$
Oh and Andino[37]	298	760	RR	9.3 ± 0.4	
	298	760	RR	8.8 ± 0.3 (9.1 ± 0.3)	
Cavalli et al[27]	298	740	RR	7.71 ± 0.85 (8.28 ± 0.85)	
Wu et al[38]	295	760	RR	8.82 ± 0.66 (8.66 ± 0.66)	
Hurley et al[26]	296	700	RR	8.86 ± 0.85	
Pang et al[12]	900-1200	760	ST	na	$3.24 \times 10^{-10}\exp(-2505/T)$
Zhou et al[22]	500-2000		Ab initio	na	G3 $6.69 \times 10^{-23} T^{3.57\pm0.10}$ $\exp((2128 \pm 98)/T)$ CCSD $2.89 \times 10^{-23} T^{3.69\pm0.16}$ $\exp((1703 \pm 150)/T)$
Seal et al[23]	200-2400		Ab initio		$(1.85 \pm 0.56) \times 10^{-23} T^{3.81\pm0.04}$ $\exp((1447 \pm 27)/T)$ [b]
McGillen et al[16]	221-381	51-216	LFP-LIF	9.68 ± 0.75	
Sarathy et al[18]			Evaluation	9.61	$(3.84 \pm 1.52) \times 10^{-21} T^{3.03\pm0.05}$ $\exp((1305 \pm 29)/T)$ [c]
Atkinson[19]			SAR	6.39	$(1.68 \pm 0.02) \times 10^{-17} T^{2}$ $\exp((414.7 \pm 9.6)/T)$ [c]
Bethel et al[20]			SAR	7.82	$(1.78 \pm 0.02) \times 10^{-17} T^{2}$ $\exp((463.0 \pm 7.5)/T)$ [c]
This work	298-715	23-135	LFP-LIF	9.00 ± 0.52	$k_1 = 1.15 \times 10^{-19} T^{2.64}$ $\exp(940/T)$

Abbreviations: FP-RF, flash photolysis with resonance fluorescence detection; LPF-LIF, laser flash photolysis/laser-induced fluorescence; PR-UV, pulsed radiolysis/UV detection; RR, relative rate; SAR, structure activity relationship; ST, shock tube.

[a] For relative rate experiments, the values reported have been updated with new recommendations if available. Values in parentheses are the original reported values.

[b] The more complex temperature parameterization of Seal et al have been parameterized in AT^n $\exp(-(E/R)/T)$ format.

[c] Site-specific data have been summed and parameterized in AT^n $\exp(-(E/R)/T)$ format.

TABLE 3 Summary of experimental conditions and bimolecular rate coefficients for the *s*-butanol and OH reaction

Temperature (K)	Pressure (Torr)	[*s*-Butanol] (molec cm^{-3})	k_2 (cm^3 $molecule^{-1}$ s^{-1})	Temperature (K)	Pressure (Torr)	[*s*-Butanol] (molec cm^{-3})	k_2 (cm^3 $molecule^{-1}$ s^{-1})
298	30	0.5-3.6	8.66 ± 0.33[a,d]	420	50	1.9-17.5	6.94 ± 0.70[c,e]
298	30	0.95-4.0	8.46 ± 0.48[a,d]	450	30	0.3-2.6	7.94 ± 0.56[b,d]
298	30	0.5-4.8	8.56 ± 0.97[a,d]	450	30	0.3-2.8	8.04 ± 0.56[b,d]
298	50	8.2-44	8.53 ± 0.16[a,e]	473	110	0.3-2.5	8.05 ± 0.81[c,d]
298	50	8.2-44	8.84 ± 0.89[a,e]	550	50	0.9-22.5	8.90 ± 0.89[c,e]
298	50	4.6-19.0	8.48 ± 0.85[a,e]	562	110	3.9-26.1	9.75 ± 0.98[c,d]
298	50	7.0-38.0	8.37 ± 0.84[a,e]	612	110	3.0-13.8	10.8 ± 1.1[b,e]
369	30	0.3-3.1	8.00 ± 0.56[c,d]	615	50	8.4-27.1	10.4 ± 1.0[c,e]
372	50	3.2-13.6	7.27 ± 0.51[c,e]	660	50	8.5-22.4	12.1 ± 1.2[c,e]
372	50	4.0-23.1	7.25 ± 0.73[c,e]	660	110	4.1-18.5	10.4 ± 1.0[c,e]
410	30	0.3-2.6	8.08 ± 0.57[b,d]	690	50	6.8-28.2	11.6 ± 1.2[c,e]

[a] Standard 1σ error.

[b] 7% error based on standard deviation of room temperature measurements.

[c] Reagent delivered by bubbler, error increased to 10%.

[d] H_2O_2 precursor.

[e] urea/H_2O_2 precursor.

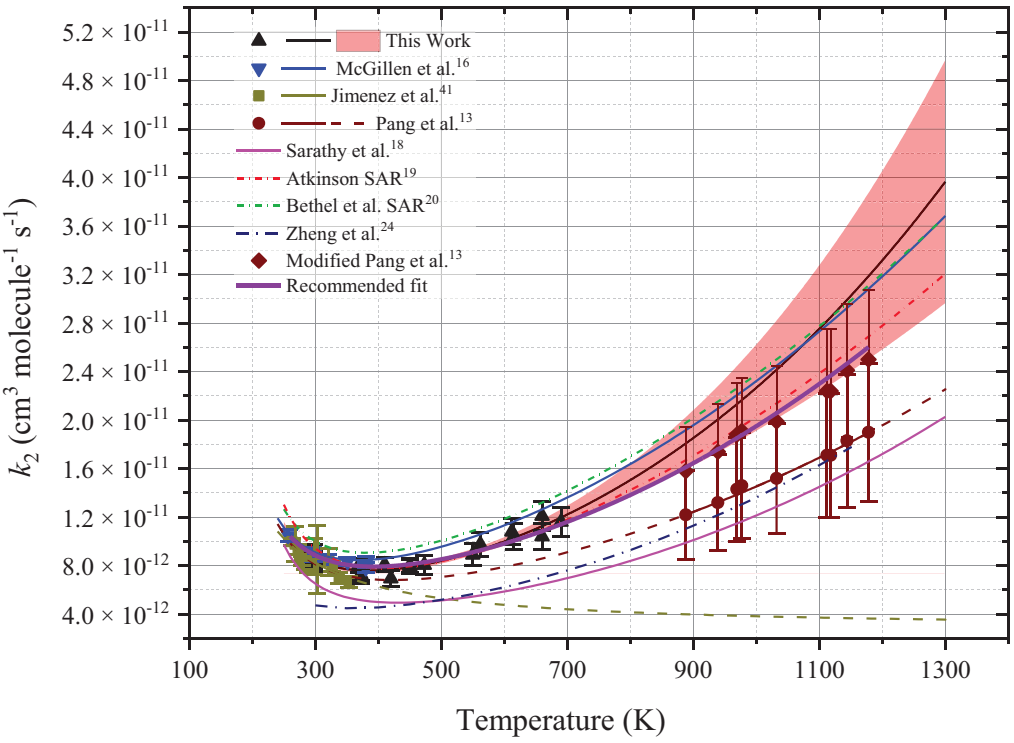

FIGURE 4 Temperature dependence for the rate coefficient for the reaction of OH and *s*-butanol incorporating this work, experimental data from Refs, 13, 16, and 41, and theoretical data from Refs. 18–20 and 24 [Color figure can be viewed at wileyonlinelibrary.com]

TABLE 4 Comparison of k_2 with literature data

Reference	Temperature (K)	Pressure (Torr)	Technique	$k_{2,298\ K}$ (cm^3 molecule^{-1} s^{-1})	$k_2(T)$ (cm^3 molecule^{-1} s^{-1})
Chew and Atkinson[39]	296	760	RR[a]	8.6 ± 2.2[a] (9.2 ± 2.4)	
Baxley and Wells[40]	297	760	RR	8.8 ± 2.2 (9.3 ± 2.3)	
	297	760	RR	7.6 ± 1.9 (8.1 ± 2.0)	
Jimenez et al[41]	263-354	41-193	LPF-LIF	8.8 ± 1.5	$(2.8 \pm 1.2) \times 10^{-12} \exp(328 \pm 124/T)$
McGillen et al[16]	221-381	51-216	LFP-LIF	9.68 ± 0.75	
Pang et al[13]	888-1178	722-942	ST	na	
Zheng et al[24]	200-2400		Ab initio		$(1.30 \pm 0.05) \times 10^{-20} T^{2.86 \pm 0.01} \exp((1017.8 \pm 3.7)/T)$[b]
Sarathy et al[18]			Evaluation	6.59	$(5.13 \pm 0.37) \times 10^{-22} T^{3.25 \pm 0.01} \exp((1417.8 \pm 6.0)/T)$[c]
Atkinson[19]			SAR	9.51	$(1.12 \pm 0.02) \times 10^{-17} T^2 \exp((609 \pm 15)/T)$[c]
Bethel et al[20]			SAR	10.1	$(1.33 \pm 0.02) \times 10^{-17} T^2 \exp((593 \pm 10)/T)$[c]
This work	298-690	30-110	LFP-LIF	8.55 ± 0.57	$1.38 \times 10^{-21} T^{3.22} \exp(1243/T)$

Abbreviations: LPF-LIF, laser flash photolysis/laser induced fluorescence; RR, relative rate; SAR, structure activity relationship; ST, shock tube.

[a]For relative rate experiments, the values reported have been updated with new recommendations if available. Values in parentheses are the original reported values.

[b]The more complex temperature parameterization of Zheng et al have been parameterized in $AT^n \exp(-(E/R)/T)$ format.

[c]Site-specific data have been summed and parameterized in $AT^n \exp(-(E/R)/T)$ format.

At lower temperatures, there is excellent agreement with the work of McGillen et al[16] and the relative rate studies of Chew and Atkinson[39] and Baxley and Wells[40] (see Table 4). Our values appear to lie slightly above the data of Jimenez et al[41] (263-354 K), who unlike, McGillen et al were able to represent their data with a simple Arrhenius expression with no evidence of upward curvature.

TABLE 5 Summary of experimental conditions and bimolecular rate coefficients for the iso-butanol and OH reaction

Temperature (K)	Pressure (Torr)	[*i*-butanol] (molec cm^{-3})	k_3 (cm^3 molecule^{-1} s^{-1})	Temperature (K)	Pressure (Torr)	[*i*-butanol] (molec cm^{-3})	k_3 (cm^3 molecule^{-1} s^{-1})
298	30	0.4-3.0	8.74 ± 0.14	450	30	0.3-1.7	9.22 ± 0.50
298	30	0.3-2.0	9.06 ± 0.18	490	30	0.2-1.8	9.10 ± 0.49
298	30	0.8-5.4	9.21 ± 0.20	509	81	9.0-16.0	9.32 ± 0.93
298	30	0.4-2.9	8.76 ± 0.28	530	30	0.3-1.5	9.24 ± 0.50
298	30	0.6-2.8	9.25 ± 0.64	540	81	9.1-21	9.68 ± 0.97
364	30	0.7-5.1	7.77 ± 0.42	551	82	14-24	9.71 ± 0.97
368	30	0.3-2.2	8.70 ± 0.47	564	81	9.0-26.0	10.1 ± 1.0
368	30	0.3-2.3	8.66 ± 0.47	587	81	8.6-19.6	10.5 ± 1.1
410	30	0.3-2.0	9.78 ± 0.53	595	82	10.2-30.0	10.5 ± 1.1
420	30	0.6-4.6	8.27 ± 0.45	607	82	15.0-24.5	11.0 ± 1.1
450	30	0.3-2.0	8.46 ± 0.46				

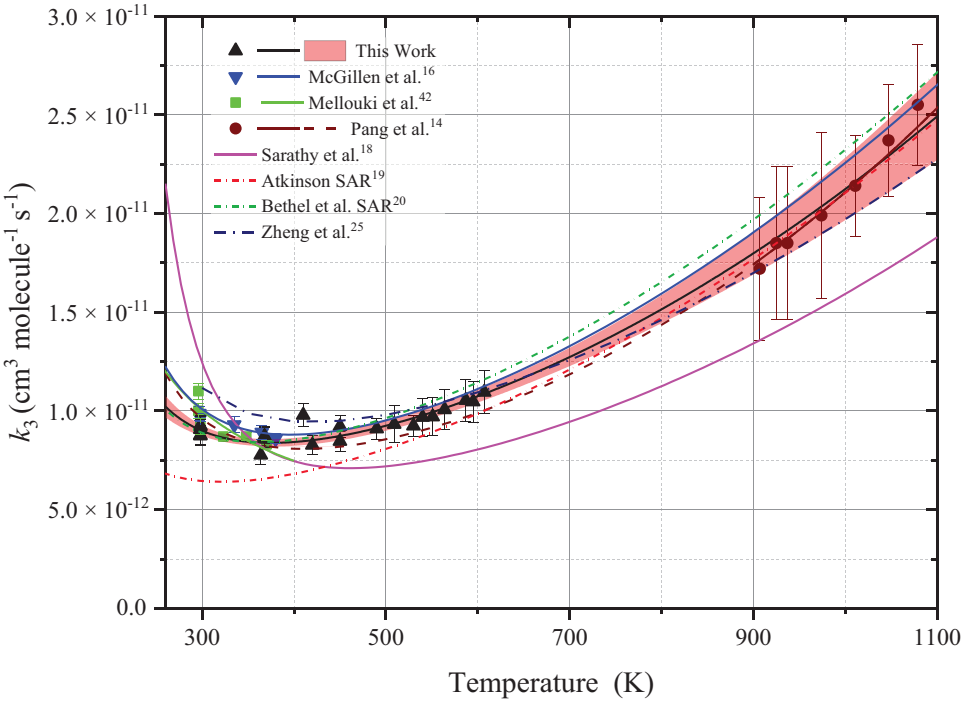

FIGURE 5 Temperature dependence for the rate coefficient for the reaction of OH and *i*-butanol incorporating this work, experimental data from Refs. 14, 16, and 42, and theoretical data from Refs. 14 and 18–20 [Color figure can be viewed at wileyonlinelibrary.com]

For *s*-butanol, there appears to be poor agreement between the experimental data in this work and the shock tube measurements of Pang et al.[13] The values of k_2 reported by Pang et al are heavily dependent on secondary modeling as discussed in the final section of the discussion.

The theoretical calculations of Zheng et al[24] for k_2 are approximately 50% lower than measured in this study or by McGillen et al but are in excellent agreement with Pang et al around 900-1200 K. The SAR predictions of Bethel et al are in good agreement, predicting a minimum in k_2 around 400 K and overestimating the current measurements by ~20%.

3.3 | *i*-Butanol

Temperature-dependent rate coefficients for the reaction of OH with *i*-butanol (k_3) are shown in Table 5 and Figure 5. Our values show a decrease in k_3 between 300 and 370 K,

TABLE 6 Comparison of k_3 with literature data

Reference	Temperature (K)	Pressure (Torr)	Technique	$k_{3,298\ K}$ (cm^3 $molecule^{-1}$ s^{-1})	$k_3(T)$ (cm^3 $molecule^{-1}$ s^{-1})
Wu et al[38]	295	760	RR[a]	9.25 ± 0.36[a] (9.08 ± 0.35)	
	295	760	RR	9.26 ± 0.43 (9.59 ± 0.45)	
Mellouki et al[42]	241-373	108	LPF-LIF	10.0 ± 1.0	$(2.8 \pm 1.2) \times 10^{-12} \exp((328 \pm 124)/T)$
	298	760	RR	9.0 8.5	
	298	760	RR	9.8	
McGillen et al[16]	224-381	60-216	LFP-LIF	9.72 ± 0.72	
Pang et al[14]	907-1147	~760	ST	Na	$1.84 \times 10^{-10} \exp(-2350/T)$ net k only
Zheng et al[25]	200-2000	na	Ab initio and TST	11.2	$(1.61 \pm 0.07) \times 10^{-21} T^{2.54 \pm 0.01} \exp((1065.8 \pm 3.8)/T)$[a]
Sarathy et al[18]			Evaluation	6.59	$(8.9 \pm 3.0) \times 10^{-24} T^{3.81 \pm 0.04} \exp((1876 \pm 25)/T)$[b]
Atkinson[19]			SAR	6.45	$(1.11 \pm 0.01) \times 10^{-17} T^2 \exp((658.6 \pm 2.7)/T)$[b]
Bethel et al[20]			SAR	8.92	$(1.31 \pm 0.01) \times 10^{-17} T^2 \exp((572.5 \pm 8.8)/T)$[b]
This work	298-607	30-82	LFP-LIF	9.01 ± 0.49	$2.05 \times 10^{-18} T^{2.20} \exp(818/T)$

Abbreviations: LPF-LIF, laser flash photolysis/laser induced fluorescence; RR, relative rate; SAR, structure activity relationship; ST, shock tube.

[a]For relative rate experiments, the values reported have been updated with new recommendations if available. Values in parentheses are the original reported values.

[b]The more complex temperature parameterization of Zheng et al have been parameterized in $AT^n \exp(-(E/R)/T)$ format.

[c]Site-specific data have been summed and parameterized in $AT^n \exp(-(E/R)/T)$ format.

beyond this minimum in k_3 around 370-420 K, k_3 gradually increases with temperature. For *i*-butanol, both the negative and positive temperature dependencies are less pronounced than for *s*-butanol.

Although there are slightly fewer studies for comparison, as detailed in Table 6, the agreement of the current work with the room temperature values,[38] the temperature-dependent studies of McGillen et al[16] and Mellouki et al[42] and the modified SAR of Bethel et al[20] is excellent. In contrast to *s*-butanol, extrapolation of our data to the temperatures of the shock tube study of Pang et al[14] appear to be in good agreement. A rationale for these observations is presented in the final discussion section. Combining the experimental work of McGillen et al and Pang et al produces the following modified Arrhenius parameterization valid from 260-1150 K:

$$k_3(T) = (5.1 \pm 5.3) \times 10^{-20} T^{2.72 \pm 0.14} \exp((1059 \pm 67)/T)\ \text{cm}^3\ \text{molecule}^{-1}\ \text{s}^{-1}.$$

The reaction has been studied theoretically most recently by Zheng et al[25] using ab initio calculations and transition state theory. As with the other calculations on reactions (1) and (2), the Truhlar group has demonstrated the importance of a careful consideration of anharmonic factors in calculating site-specific rate coefficients with low or negative barriers. These calculations successfully predict the change from negative to positive temperature dependence for R1-R3.

3.4 | *t*-Butanol

Details on the reaction of OH with *t*-butanol are in Sime[43] and will be presented in a subsequent paper that includes direct measurements of the β-hydroxyperoxy decomposition to regenerate OH. To allow comparisons on OH reactivity with other butanols, we summarize the temperature dependence of reaction 4 in Figure 6.

In contrast to the other butanols, the room temperature rate coefficient is approximately an order of magnitude smaller and the temperature dependence above 300 K is entirely positive and there appears to be good agreement with the direct measurements on R4, obtained via isotope studies, by Stranic et al.[15] The above data on k_4 can be parameterized to give:

$$k_4(T) = (8.8 \pm 10.4) \times 10^{-22} T^{3.24 \pm 0.15} \exp((711 \pm 83)/T)\ \text{cm}^3\ \text{molec}^{-1}\ \text{s}^{-1}.$$

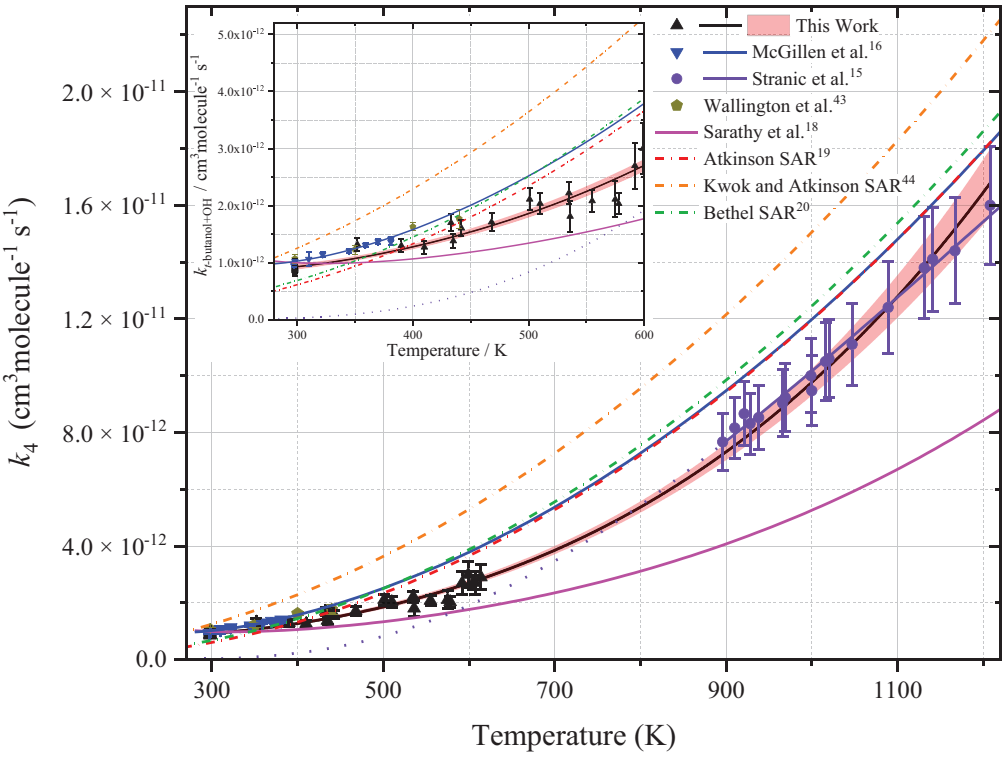

FIGURE 6 Temperature dependence for the rate coefficient for the reaction of OH and *t*-butanol. Experimental data from this work (black triangles, McGillen et al[16] (blue inverted triangles) Stranic et al[15] and Wallington et al[44] (green pentagons). Also shown are SAR predictions from Atkinson,[19] Kwok and Atkinson,[45] and Bethel et al[20] and the parameterization of Sarathy et al[18] The inset provides an expansion of the lower temperature data where the symbols retain their meanings from the main figure [Color figure can be viewed at wileyonlinelibrary.com]

3.5 | Comparison of rate coefficients, implications on branching ratios and the fate of β-hydroxyperoxy radicals

The most obvious difference between the overall rate coefficients of the butanols is that R4, the reaction of OH and *t*-butanol, is significantly smaller at room temperature, shows only a positive temperature dependence and that the positive temperature dependence is stronger than for the other butanols. This is entirely consistent with OH having to abstract from the relatively strong primary β C−H bonds or from the O−H bond. In contrast to most of the abstractions in the other butanols, these processes are predicted to have positive barriers.

Despite, having different numbers and types of α, β, γ, and δ C−H bonds, the room temperature rate coefficients of *n*, *s*, and *i*-butanol are remarkably similar. The limited product studies, predominantly at room temperature, suggest that abstraction at the α position dominates at 298 K, but the studies of Truhlar and coworkers[23-25] have emphasized that the way that barrier heights and anharmonicity effects combine to determine branching ratios is complex and branching ratios will change as a function of temperature. Further product studies are required, particularly at lower temperatures (~200 to 300 K) where the studies of Truhlar and coworkers suggest that branching ratios should change substantially with α abstractions no longer dominating.

Although this work only determines total removal rate coefficients, comparison with the studies of Pang et al[12-14] do allow us to draw conclusions on β abstraction pathways and the fate of the resultant β-hydroxyperoxy radicals. As discussed in the Introduction, decomposition of the β-hydroxyperoxy radical will be very rapid under shock tube conditions with a fraction of the decompositions regenerating OH. Pang et al were aware that they were only measuring the net OH removal rate and made use of modeling studies and calculations from other groups to generate the total removal rate coefficients.

Let us start by looking at the reaction of OH with *i*-butanol (R3). Here there is only a single β channel (abstraction at the tertiary C−H bond) and experimental, SAR,[20] evaluations,[16] and calculations[25] all agree that this branching ratio is ~0.2 leading to the $(CH_3)_2CCH_2OH$ hydroperoxy radical. Once again calculations are in agreement that reaction R7a dominates for the decomposition

of this species:

$$(CH_3)_2CCH_2OH \rightarrow OH + (CH_3)_2C = CH_2 \quad \text{(R7a)}$$

$$\rightarrow H + (CH_3)_2C = CHOH \quad \text{(R7b)}$$

Pang et al[14] were therefore able to accurately convert their net measurements of R3 into overall rate coefficients, and these values are in excellent agreement with the extrapolations of this work (where there is no significant β decomposition) as can be seen in Figure 5. This good agreement confirms the accuracy of the β branching ratio for the shock tube region.

The situation is quite different for *s*-butanol (R2). Examination of Figure 4 shows that our measured value of k_2 at ~600 K is already equal to the proposed value of k_2 at ~900 K. For the β-hydroxyperoxy arising from *i*-butanol OH regenerating was in competition with C−H bond cleavage that has a significantly higher barrier. However for the β-hydroxyperoxy arising from *s*-butanol, OH regeneration is in competition with C−C bond cleavage that has a lower barrier than C−H cleavage. Pang et al[13] modeled their overall k_2 based on modified models from Frassoldati et al,[46] Hansen et al,[47] and Sarathy et al.[18] Each of these models has a different branching ratio for β abstraction and deals differently with the decomposition of the resulting β-hydroxyperoxy radicals:

$$CH_3CHCH(OH)CH_3 \rightarrow OH + CH_3CH = CHCH_3 \quad \text{(R8a)}$$

$$\rightarrow CH_3 + CH_3CH = CHOH \quad \text{(R8b)}$$

$$CH_3CH_2CH(OH)CH_2 \rightarrow OH + CH_3CH_2CH = CH_2 \quad \text{(R9a)}$$

$$\rightarrow C_2H_5 + CH_2 = CHOH \quad \text{(R9b)}$$

There are several differences between the mechanisms. The Hansen et al mechanism uses a value for k_2 that is almost an order of magnitude too slow; however, the main differences refer to the fraction of k_2 leading to β abstraction and then, more significantly, the fate of the β-hydroxyperoxy radicals with the Sarathy et al and Frassoldati et al mechanisms favoring the elimination of the methyl radical. Pang et al[13] tabulated the values of k_2 for each mechanism and as shown in Figure 4, the mechanism of Hansen et al[47] (~38% production of β-hydroxyperoxy radicals with ~80% OH regeneration) is in good agreement with the extrapolation of the current measurements. This OH yield of ~30% could of course be made up of a variety of combinations of branching ratios. However, the high yield of OH regeneration from the β-hydroxyperoxy is consistent with measurements from the β-hydroxyperoxy radical produced from reaction 4. Zheng et al[24] calculate a total branching ratio to β-hydroxyperoxy of 47% in reasonable agreement with our observations. We recommend the following parameterization based on the current work, the low-temperature studies of McGillen et al and the data of Pang et al[13] interpreted with the Hansen mechanism:

$$k_2(T) = (3.5 \pm 3.0) \times 10^{-20} T^{2.76 \pm 0.12} \exp((1085 \pm 55)/T) \ \text{cm}^3 \ \text{molec}^{-1} \ \text{s}^{-1}.$$

For the β-hydroxyperoxy radical produced from R1b, again two channels are possible:

$$CH_3CH_2CHCH_2OH \rightarrow OH + 1\text{−butene} \quad \text{(R5a)}$$

$$\rightarrow CH_3 + CH_2 = CHCH_2OH. \quad \text{(R5b)}$$

However, there is also an additional source of OH from the δ abstraction:

$$CH_2CH_2CH_2CH_2OH \rightarrow OH + 2C_2H_4. \quad \text{(R10)}$$

Pang et al[12] modeled their shock tube data based around the calculated branching ratios of Zhou et al[22] (8% for β abstraction and 34% for δ abstraction) with OH regeneration from the δ hydroxyperoxy radical at 85% and at 17% for the β-hydroxyperoxy radical giving an overall OH generation of 30%. Figure 3 shows the overall rate coefficients from Pang et al are in good agreement with the extrapolation of our current work suggesting that the overall OH regeneration yield is correct, but the mechanism for β-hydroxyperoxy radical decomposition is different. The high yield of the δ-hydroxyperoxy radical is surprising and does not match either the evaluation of McGillen et al[16] ($\beta = 19\%$, $\delta = 14\%$) or the more recent calculations of Seal et al[23] ($\beta = 18\%$, $\delta = 8\%$) for the shock tube temperature regime. However, if OH regeneration is the dominant process from both β and δ-hydroxyperoxy radicals, then the OH yield should be somewhere between 0.25 and 0.33, in good agreement with the observations.

4 | CONCLUSIONS

The rate coefficients for the reactions of OH with *n*, *s*, and *i*-butanol have been measured over temperature ranges relevant to the onset of low-temperature combustion. The values measured provide a clear link between the negative temperature dependence of lower temperature measurements (~250 to 350 K)[16,42] and the positive

temperature dependence of the rate coefficients determined from shock tube measurements (~900 to 1200 K).[12-15] Data from 250 to 1200 K have been combined and fit with modified Arrhenius parameters to provide accurate and precise data for modeling studies. The low-temperature combustion behavior of butanols is strongly dependent on the branching ratios of the initial abstractions from butanol[48,49] and calculations are likely to provide the best information on these, particularly at higher temperatures. The current data provide a good test of ab initio and transition state calculations for systems with low or negative barriers.

Although only the total rate coefficient has been measured in this study, comparison of this work with the shock tube measurements of Pang et al[12-14] are able to shed light on the degree of OH regeneration, which primarily occurs from abstraction at the β position. Our analysis is broadly consistent with the branching ratio evaluations of McGillen et al[16] and the theoretical calculations of Truhlar and coworkers.[23-25] The analysis also suggests that OH is the major product from the decomposition of β-hydroxperoxy radicals (with alkene coproduct), whereas the mechanisms of Sarathy et al[18] and Frassoldati et al[46] have alkyl radical elimination (mainly CH_3) with enol as the coproduct.

ACKNOWLEDGMENTS

SLS is grateful for a studentship from the EPSRC doctoral training programme in Bioenergy.

ORCID

Paul W. Seakins https://orcid.org/0000-0002-4335-8593

REFERENCES

1. Tao L, Tan ECD, McCormick R, et al. Techno-economic analysis and life-cycle assessment of cellulosic isobutanol and comparison with cellulosic ethanol and n-butanol. *Biofuels Bioprod Biorefining*. 2014;8:30-48.
2. Creutzig F, Ravindranath NH, Berndes G, et al. Bioenergy and climate change mitigation: an assessment. *GCB Bioenergy*. 2015;7:916-944.
3. Bergthorson JM, Thomson MJ. A review of the combustion and emissions properties of advanced transportation biofuels and their impact on existing and future engines. *Renewable Sustainable Energy Rev*. 2015;42:1393-1417.
4. Kumar BR, Saravanan S. Use of higher alcohol biofuels in diesel engines: a review. *Renewable Sustainable Energy Rev*. 2016;60:84-115.
5. Trindade WRD, dos Santos RG. Review on the characteristics of butanol, its production and use as fuel in internal combustion engines. *Renewable Sustainable Energy Rev*. 2017;69:642-651.
6. Veza I, Said MFM, Latiff ZA. Improved performance, combustion and emissions of SI engine fuelled with butanol: a review. *Int J Automot Mech Eng*. 2020;17:7648-7666.
7. Shirazi SA, Abdollahipoor B, Windom B, Reardon KF, Foust TD. Effects of blending C3-C4 alcohols on motor gasoline properties and performance of spark ignition engines: a review. *Fuel Process Technol*. 2020;197:20.
8. Agarwal AK, Singh AP, Maurya RK. Evolution, challenges and path forward for low temperature combustion engines. *Prog Energy Combust Sci*. 2017;61:1-56.
9. Pilling MJ, Robertson SH, Seakins PW. Elementary radical reactions and autoignition. *J Chem Soc, Faraday Trans*. 1995;91:4179-4188.
10. Zador J, Taatjes CA, Fernandes RX. Kinetics of elementary reactions in low-temperature autoignition chemistry. *Prog Energy Combust Sci*. 2011;37:371-421.
11. Westbrook CK. *Ann Rev Phys Chem*. 2013:201-219.
12. Pang GA, Hanson RK, Golden DM, Bowman CT. Rate constant measurements for the overall reaction of OH+1-butanol →. *J Phys Chem A*. 2012;116:2475-2483.
13. Pang GA, Hanson RK, Golden DM, Bowman CT. Experimental determination of the high-temperature rate constant for the reaction of OH with sec-butanol. *J Phys Chem A*. 2012;116:9607-9613.
14. Pang GA, Hanson RK, Golden DM, Bowman CT. High-temperature rate constant determination for the reaction of OH with iso-butanol. *J Phys Chem A*. 2012;116:4720-4725.
15. Stranic I, Pang GA, Hanson RK, Golden DM, Bowman CT. Shock tube measurements of the t-butanol plus OH reaction rate and the t-C_4H_8OH radical beta-scission branching ratio using isotopic labeling. *J Phys Chem A*. 2013;117:4777-4784.
16. McGillen MR, Baasandorj M, Burkholder JB. Gas-phase rate coefficients for the OH plus n-, i-, s-, and t-butanol reactions measured between 220 and 380 K: non-Arrhenius behavior and site-specific reactivity. *J Phys Chem A*. 2013;117:4636-4656.
17. Mu YJ, Mellouki A. Temperature dependence for the rate constants of the reaction of OH radicals with selected alcohols. *Chem Phys Lett*. 2001;333:63-68.
18. Sarathy SM, Vranckx S, Yasunaga K, et al. A comprehensive chemical kinetic combustion model for the four butanol isomers. *Combust Flame*. 2012;159:2028-2055.
19. Atkinson R. A structure-activity relationship for the estimation of rate constants for the gas-phase reactions of oh radicals with organic-compounds. *Int J Chem Kinet*. 1987;19:799-828.
20. Bethel HL, Atkinson R, Arey J. Kinetics and products of the reactions of selected diols with the OH radical. *Int J Chem Kinet*. 2001;33:310-316.
21. Galano A, Alvarez-Idaboy JR, Bravo-Perez G, Ruiz-Santoyo ME. Gas phase reactions of C1-C4 alcohols with the OH radical: a quantum mechanical approach. *PCCP*. 2002;4:4648-4662.
22. Zhou CW, Simmie JM, Curran HJ. Rate constants for hydrogen-abstraction by OH from n-butanol. *Combust Flame*. 2011;158:726-731.
23. Seal P, Oyedepo G, Truhlar DG. Kinetics of the hydrogen atom abstraction reactions from 1-butanol by hydroxyl radical: theory matches experiment and more. *J Phys Chem A*. 2013;117:275-282.
24. Zheng JJ, Oyedepo GA, Truhlar DG. Kinetics of the hydrogen abstraction reaction from 2-butanol by OH radical. *J Phys Chem A*. 2015;119:12182-12192.
25. Zheng JJ, Meana-Paneda R, Truhlar DG. Prediction of experimentally unavailable product branching ratios for biofuel

combustion: the role of anharmonicity in the reaction of isobutanol with OH. *J Am Chem Soc*. 2014;136:5150-5160.
26. Hurley MD, Wallington TJ, Lauirsen L, et al. Atmospheric chemistry of n-butanol: kinetics, mechanisms, and products of Cl atom and OH radical initiated oxidation in the presence and absence of NOx. *J Phys Chem A*. 2009;113:7011-7020.
27. Cavalli F, Geiger H, Barnes I, Becker KH. FTIR kinetic, product, and modeling study of the OH-initiated oxidation of 1-butanol in air. *Environ Sci Technol*. 2002;36:1263-1270.
28. Speak TH, Blitz MA, Stone D, Seakins PW. A new instrument for time-resolved measurement of HO_2 radicals. *Atmos Meas Technol*. 2020;13:839-852.
29. Dunlop JR, Tully FP. Catalytic dehydration of alcohols by OH—2-propanol—an intermediate case. *J Phys Chem*. 1993;97:6457-6464.
30. Carr SA, Blitz MA, Seakins PW. Site-specific rate coefficients for reaction of OH with ethanol from 298 to 900 K. *J Phys Chem A*. 2011;115:3335-3345.
31. Carr SA, Still TJ, Blitz MA, et al. Experimental and theoretical study of the kinetics and mechanism of the reaction of OH radicals with dimethyl ether. *J Phys Chem A*. 2013;117:11142-11154.
32. Stone D, Au K, Sime S, et al. Unimolecular decomposition kinetics of the stabilised Criegee intermediates CH_2OO and CD_2OO. *PCCP*. 2018;20:24940-24954.
33. Whelan CA, Blitz MA, Shannon R, et al. Temperature and pressure dependent kinetics of QOOH decomposition and reaction with O_2: experimental and theoretical investigations of QOOH radicals derived from Cl + $(CH_3)_3COOH$. *J Phys Chem A*. 2019;123:10254-10262.
34. Potter DG, Blitz MA, Seakins PW. A generic method for determining r + O_2 rate parameters via OH regeneration. *Chem Phys Lett*. 2019;730:213-219.
35. Wallington TJ, Kurylo MJ. The gas-phase reactions of hydroxyl radicals with a series of aliphatic-alcohols over the temperature-range 240-440-K. *Int J Chem Kinet*. 1987;19:1015-1023.
36. Nelson L, Rattigan O, Neavyn R, Sidebottom H, Treacy J, Nielsen OJ. Absolute and relative rate constants for the reactions of hydroxyl radicals and chlorine atoms with a series of aliphatic-alcohols and ethers at 298 K. *Int J Chem Kinet*. 1990;22:1111-1126.
37. Oh S, Andino JM. Kinetics of the gas-phase reactions of hydroxyl radicals with C1-C6 aliphatic alcohols in the presence of ammonium sulfate aerosols. *Int J Chem Kinet*. 2001;33:422-430.
38. Wu H, Mu YJ, Zhang XS, Jiang GB. Relative rate constants for the reactions of hydroxyl radicals and chlorine atoms with a series of aliphatic alcohols. *Int J Chem Kinet*. 2003;35:81-87.
39. Chew AA, Atkinson R. OH radical formation yields from the gas-phase reactions of O_3 with alkenes and monoterpenes. *J Geophys Res-Atmos*. 1996;101:28649-28653.
40. Baxley JS, Wells JR. The hydroxyl radical reaction rate constant and atmospheric transformation products of 2-butanol and 2-pentanol. *Int J Chem Kinet*. 1998;30:745-752.
41. Jimenez E, Lanza B, Garzon A, Ballesteros B, Albaladejo J. Atmospheric degradation of 2-butanol, 2-methyl-2-butanol, and 2,3-dimethyl-2-butanol: OH kinetics and UV absorption cross sections. *J Phys Chem A*. 2005;109:10903-10909.
42. Mellouki A, Oussar F, Lun X, Chakir A. Kinetics of the reactions of the OH radical with 2-methyl-1-propanol, 3-methyl-1-butanol and 3-methyl-2-butanol between 241 and 373 K. *PCCP*. 2004;6:2951-2955.
43. Sime SL. *Kinetic studies of bio-butanol oxidation under low temperature combustion conditions* (PhD thesis). University of Leeds, Leeds, UK; 2019
44. Wallington TJ, Dagaut P, Liu RZ, Kurylo MJ. Gas-phase reactions of hydroxyl radicals with the fuel additives methyl tert-butyl ether and tert-butyl alcohol over the temperature-range 240-K to 440-K. *Environ Sci Technol*. 1988;22:842-844.
45. Kwok ESC, Atkinson R. Estimation of hydroxyl radical reaction-rate constants for gas-phase organic-compounds using a structure-reactivity relationship—an update. *Atmos Environ*. 1995;29:1685-1695.
46. Frassoldati A, Grana R, Faravelli T, Ranzi E, Osswald P, Kohse-Hoinghaus K. Detailed kinetic modeling of the combustion of the four butanol isomers in premixed low-pressure flames. *Combust Flame*. 2012;159:2295-2311.
47. Hansen N, Harper MR, Green WH. High-temperature oxidation chemistry of n-butanol—experiments in low-pressure premixed flames and detailed kinetic modeling. *PCCP*. 2011;13:20262-20274.
48. Merchant SS, Zanoelo EF, Speth RL, Harper MR, Van Geem KM, Green WH. Combustion and pyrolysis of iso-butanol: experimental and chemical kinetic modeling study. *Combust Flame*. 2013;160:1907-1929.
49. Agbro E, Tomlin AS. Low temperature oxidation of n-butanol: key uncertainties and constraints in kinetics. *Fuel*. 2017;207:776-789.

How to cite this article: Sime SL, Blitz MA, Seakins PW. Rate coefficients for the reactions of OH with butanols from 298 K to temperatures relevant for low-temperature combustion. *Int J Chem Kinet*. 2020;1-14.
https://doi.org/10.1002/kin.21422